ELSEVIER

Nuclear Instruments and Methods in Physics Research B 164–165 (2000) 44–52

NIM B
Beam Interactions with Materials & Atoms

www.elsevier.nl/locate/nimb

In-flight annihilation during positron channeling

A.W. Hunt [a,b,*], D.B. Cassidy [a,b], F.A. Selim [c], R. Haakenaasen [d], T.E. Cowan [b], R.H. Howell [b], K.G. Lynn [e], J.A. Golevchenko [a]

[a] *Department of Physics, Harvard University, Cambridge, MA 02138, USA*
[b] *Lawrence Livermore National Laboratory, 7000 East Avenue, L-280, Livermore, CA 94551, USA*
[c] *Engineering Physics Department, Alexandria University, Alexandria 21544, Egypt*
[d] *Norwegian Defense Research Establishment, 2027 Kjeller, Norway*
[e] *Department of Physics, Washington State University, Pullman, WA 99164-2814, USA*

Abstract

Energetic positrons propagating along low index directions in a crystal interact strongly with the periodic array of atoms via a process known as channeling. The trajectories of such channeled positrons can be manipulated to sample different spatial regions in the crystal. Here we report the first observations of channeling effects on in-flight annihilation radiation from positrons traversing a thin gold crystal. The channeling minimum yield for two-photon annihilation is shown to be significantly enhanced compared to single photon annihilation due to the selective interaction of well-channeled positrons with valence electrons in the interstitial regions of the crystal. Both classical and quantum calculation of annihilation yields are compared to the experimental data.

1. Introduction

The channeling phenomenon has been extensively studied since its 'discovery' in the 1960s [1–5]. Materials analysis using ion channeling is now well established at many laboratories around the world [6]. The most common technique is to examine the energy distribution of ions backscattered from a beam penetrating a material close to a major crystallographic direction. By considering the ion energy loss, the crystalline quality of thin films can be depth analyzed in a simple manner [7,8]. Furthermore, the use of channeled charged particles gives the experimenter the unique ability to control the spatial distribution in the interstices. This ability has been exploited to probe the lattice site of implanted and intrinsic impurities in crystalline solids [9,10].

When positive ions channel, they are focused into the crystal's interstitial regions by a series of highly correlated small angle scattering events. This focusing suppresses backscattering (and indeed all close nuclear collision processes) with the lattice and increases backscattering from any impurities residing in the interstitial regions. Moreover, the regions sampled by the channeled ions can be controlled on an atomic scale simply by changing the angle of the incident beam. As this

* Corresponding author. Present address: Center for Materials Research, Washington State University, Pullman, WA 99164-2711, USA. Tel.: 509-335-3222; fax: 509-335-4145.
E-mail address: alwhunt@wsu.edu (A.W. Hunt).

0168-583X/00/$ - see front matter
PII: S0168-583X(99)01004-6

deviates from that of the low-index crystal direction the ion-momentum transverse to this direction increases, and the trajectories penetrate closer to the atomic nuclei of the lattice. Thus, when observing the backscattering angular yield, a characteristic channeling dip is obtained for the lattice nuclei while a peak is obtained from any interstitial impurities [9].

Interstitial flux peaking also means that electron interactions occur primarily with loosely bound valence electrons. This decreases the ion energy loss [11,12] and thereby increases the range of channeled ions which arguably was the first experimental evidence of the channeling effect [13]. This reduction of core electron interactions has been used to study unique interactions of highly stripped ions with a quasi-free electron gas [14,15]. It has also been suggested that channeled positrons could be used to selectively probe these valence electrons [16–19].

Most positron channeling studies to date have observed the transmitted or scattered positrons in order to shed light on the applicability of channeling theory for low mass particles [16,20–23]. Axially channeled positrons exhibit strikingly similar channeling characteristics to those of heavy ions [20]. This suggests that a new probe can be developed that uses the channeling process to specify which atomic regions are sampled by the positron trajectories, while the radiation from the two-photon in-flight annihilation process would provide an experimental signal that reflects the electron properties in the sampled region. In-flight positron annihilation is sensitive to at least three electron properties. First, the annihilation rate depends on the local electron density sampled by the positrons. Second, as in thermalized positron–electron annihilation, the energy distribution of the emitted γ-rays is broadened by the electron momentum. Finally, the annihilation cross-section is spin dependent [24] and with a highly polarized positron beam electronic spin states can in principal be probed.

Such channeled positron experiments are currently very difficult compared to annihilation experiments with thermalized positrons (which have been extensively utilized to probe condensed matter systems [25–29]). While channeled positrons have the advantage of spatial wave functions that can be experimentally controlled, practical implementation requires an MeV monoenergetic positron beam with $\sim 10^7$ e^+/s. While such a beam is currently not available, the recently constructed 3 MeV monoenergetic positron beamline at Lawrence Livermore National Laboratory has sufficient flux ($\sim 10^5$ e^+/s) to demonstrate the dramatic new annihilation effects expected from channeled positron experiments. In this paper we report observations of single and two-photon annihilation for channeled positrons. Comparison of these two annihilation modes demonstrates the ability of channeled positrons to selectively sample valence electrons in the crystal. Classical and quantum theory calculations will also be compared to the experimental results.

2. Positron beamline

The experiments were performed using a 3 MeV Pelletron accelerator that was originally designed for electron acceleration. In order to accelerate positrons the polarity was switched and the electron gun in the terminal was replaced. The new gun accommodates a 109 mCi ^{22}Na positron source, a tungsten moderator, as well as appropriate focusing optics that deliver a 2 mm diameter beam to the entrance of the first accelerating section [30]. The terminal voltage was brought to 2.65 MV and stabilized by a corona current feedback system that maintained the terminal within 0.4% of the operating value [31].

Upon exiting the accelerator the beam was focused by a solenoid lens into the center of the first 90° bending magnet. The focal point was chosen to be the center to minimize the astigmatism from the magnet. All remaining astigmatism were corrected by a quadrupole located immediately after the bend. The beam was then focused by another solenoid lens at the focal point of a second 90° bending magnet where an 8 mm beam spot was defined by a collimator. After the second bend the beam went through an 8 mm active collimator before reaching the final focusing solenoid which was 3.5 m from the target. Before reaching the target area, Fig. 1, the positrons passed through a

final pair of collimation slits that defined the angular divergence and spatial size of the beam on target.

Typical beam characteristics on target were 200,000 e^+/s in a 3 mm diameter spot, with a maximum angular divergence of 0.25° and an energy spread of less then 0.4% of the beam energy. The target was a 0.6 μm thick ⟨1 1 0⟩ oriented free standing gold crystal grown at the University of Aarhus with a surface minimum yield of 3% for 2 MeV α-particles. The planer diameter of the crystal (5 mm) was only 2 mm larger than the beam spot and therefore it was necessary to house the crystal in a target holder made of scintillating material. The holder had a 4.5 mm hole and was directly coupled to a Hamamatsu R5600U ultra-compact photomultiplier tube inside the vacuum chamber. The signal from this scintillator allowed the beam to be optimized and monitored during the experiment. Also there was a beam 'halo' of about 0.3% of the total current that hit the target holder. This was the major source of background but as will be discussed below, use of the scintillator allowed this signal to be identified and easily subtracted.

Behind the target was a large angle scattering scintillator that detected positrons scattered between 10° and 20°. This detector was used in aligning the crystal and to measure the large angle scattering yield. Further downstream a 75° bending magnet deflected the transmitted positrons to a well-shielded beam dump. This was a specially designed double focusing magnet with a 10° vertical and horizontal acceptance angle. Multiple scattering measurements and calculations predicted an angular divergence of half this value, assuring efficient collection of the transmitted beam [30]. A scintillation detector used for normalization was positioned in the focal plane of the 75° magnet.

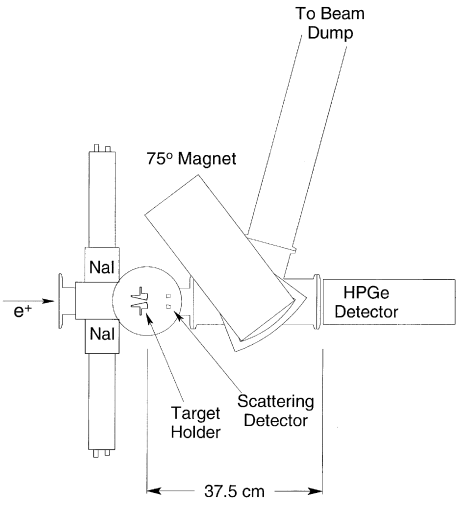

Fig. 1. Schematic diagram of the target area of the 3 MeV monoenergetic positron beamline at Lawrence Livermore National Laboratory.

3. Positron annihilation and detection

The vast majority of positrons channeling through the crystal were transmitted to the beam dump scintillator and approximately 1.5% were scattered into the large angle detector. Even fewer still (7×10^{-3}%) annihilated in-flight by single or two-photon annihilation. In the single photon annihilation process a monoenergetic γ-ray is emitted with the nucleus recoiling to conserve momentum. The energy of the photon, E_s, is given by

$$E_s = 2mc^2 + T_+ - |E_b|, \quad (1)$$

where mc^2 is the rest mass energy of the electron, T_+ the positron kinetic energy and E_b the electron binding energy. In principal each electron shell can be distinguished because the binding energy shifts the energy of the annihilation γ-ray. In practice the cross-section is too small for the single photon annihilation process to be detectable for all but the most tightly bound electrons [32].

Unlike single photon annihilation, the two-photon annihilation process does not require a nuclear recoil and can therefore occur with all electrons in the target material. The two emitted photons are coincident in time and have energies that strongly depend on the angle of emission. If the electron momentum is neglected and the positron momentum is assumed to be fixed in the direction of the beam (a good approximation for thin targets), the photon energies are given by

$$E = \frac{mc^2}{1 - \frac{cp_+}{T_+ + 2mc^2}\cos\theta}. \quad (2)$$

Here p_+ is the positron momentum and θ is the angle between the emitted photon and the beam. For 2.65 MeV positrons, the photon energies range from 276 keV for 180° emission to 3396 keV for 0° emission. Inclusion of the electron momentum further broadens the photon energy distribution.

To simultaneously detect both single and two-photon annihilation, a multiple γ-ray spectroscopy system consisting of a 7.3 cm diameter high purity germanium (HPGe) detector and two 3″ NaI scintillators was constructed. The HPGe detector was placed in the forward direction 37.5 cm from the target and subtended a half angle of 5.6°, see Fig. 1. It had a relative efficiency of 9.1×10^{-5} at 2734 keV and 7.0×10^{-5} at 3218 keV in the experimental geometry. From Eq. (2), the two-photon annihilation γ-rays that strike this detector are constrained between 3300 and 3396 keV. Curve A of Fig. 2 shows an energy spectra obtained from the HPGe detector. The demonstration spectra shown in Figs. 2 and 3 were obtained using a 3.6 μm amorphous gold foil for enhanced statistics. Single photon annihilation is easily identified; the K-shell ($|E_b| = 81$ keV), L-shell ($|E_b| = 13$ keV) and M-shell ($|E_b| = 2.6$ keV) annihilation events

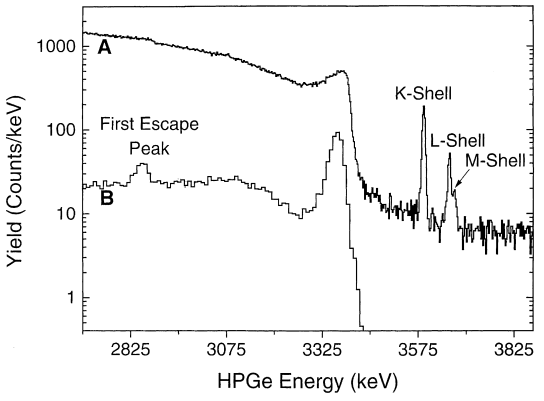

Fig. 2. HPGe energy spectra from 2.65 MeV positrons impinging on a 3.6 μm polycrystalline gold foil. (A) No coincident photon required. (B) Coincident photon required within 30 ns in one of the 3″ detectors.

are seen at 3591, 3659 and 3670 keV, respectively. The edge at 3390 keV is from the most forward directed of the two-photon annihilation γ-rays. The rising background below 3300 keV arises from positrons that strike a chamber wall and then annihilate in-flight.

The background for two-photon annihilation can be dramatically reduced by requiring the detection of both emitted γ-rays. The two NaI scintillators were placed on either side of the target chamber 8.9 cm in front of the target, collecting photons emitted between 142° and 163°. These detectors recorded the coincident ~300 keV photons emitted with the forward γ-rays that hit the HPGe detector. The signals from all detectors were routed to a multiple parameter data acquisition system that recorded energy and time information for each detector on an event by event basis. A two-dimensional histogram is presented in Fig. 3 with a 30 ns coincidence window. The horizontal and vertical axes are the photon energies recorded by the HPGe (E_{Ge}) and NaI (E_{Na}) detectors, respectively. The histogram bins are color coded with white corresponding to 0–4 counts and yellow to more than 125 counts. The two-photon annihilation peak is located at $[3370, 300]$ keV ($[E_{Ge}, E_{Na}]$). The 'tail' below the peak that extends along $E_{Na} = 300$ keV and ends at $E_{Ge} = 3270$ keV is due to γ-rays Compton scattering out of the HPGe detector. Also along this tail, the single and double escape peaks are seen at $[2859, 300]$ and $[2348, 300]$ keV from recombining positron–electron pairs created in the detector. Photons recorded in this region nevertheless represent valid two-photon annihilation events and their inclusion significantly improves the statistics in our channeling studies. Therefore, when calculating the two-photon annihilation yield all events inside the box in Fig. 3 were counted. Finally, to demonstrate the dramatic background reduction, a projection of the two-dimensional histogram onto the E_{Ge} axis is shown in Fig. 2 curve B.

4. Results

The Au crystal was first aligned by locating the four planes that intersect at the ⟨1 1 0⟩ axis. This

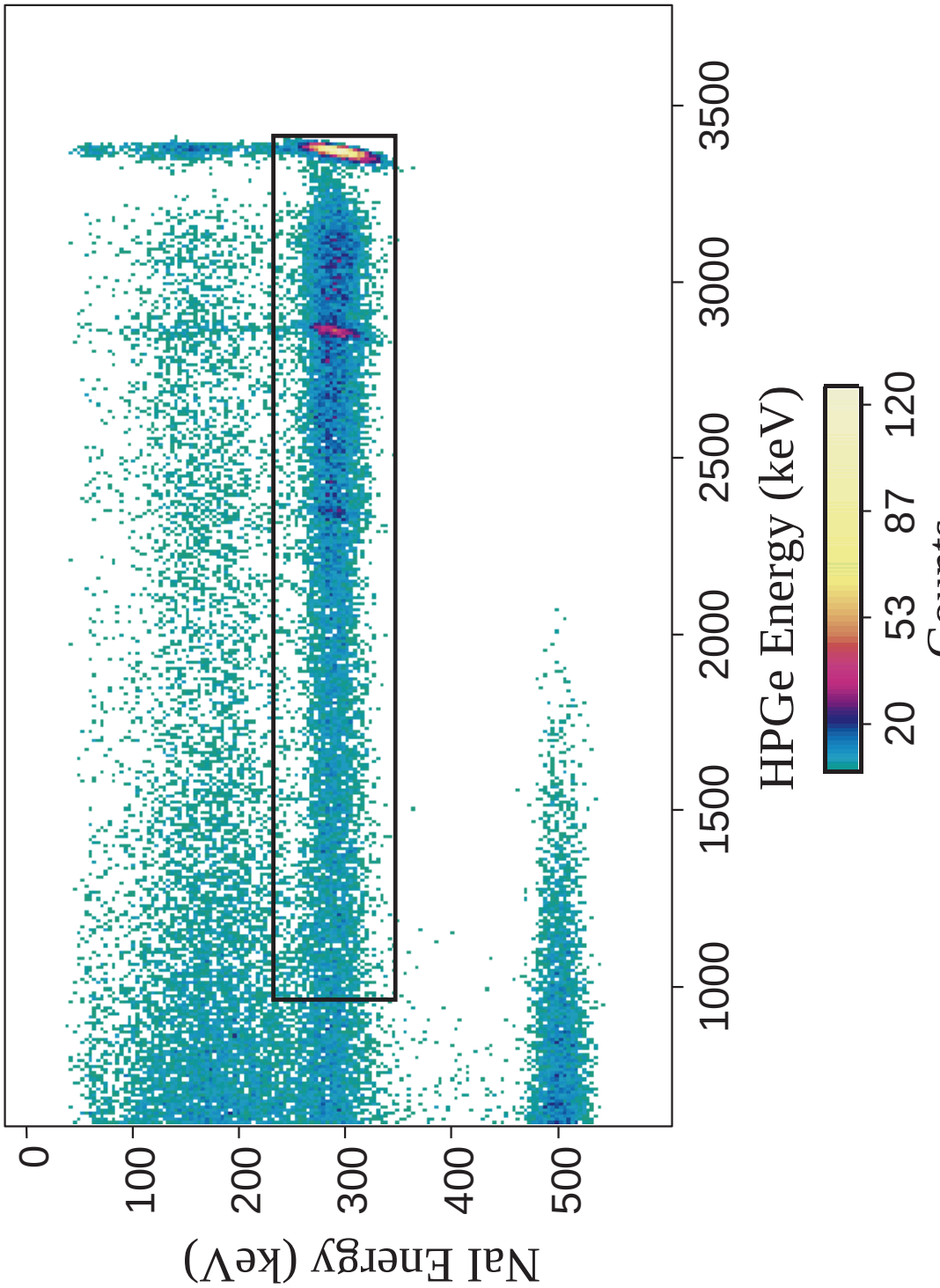

Fig. 3. Two-dimensional energy histogram from 2.65 MeV positrons impinging on a 3.6 μm polycrystalline gold foil. The horizontal and vertical axes are the energies from the HPGe (E_{Ge}) and NaI (E_{Na}) detectors, respectively. The histogram bins are color coded with white corresponding to 0–4 counts and yellow more than 125 counts.

procedure was carried out by using the planar dips in the large angle scattering detector. Counting times of ~2 s per point was sufficient which resulted in ~1000 and ~8000 counts per point in the aligned and random direction, respectively. More careful large angle scattering scans were then carried out with counting times of 10 s. Spectra with and without a coincident requirement were then taken simultaneously at 13 different angles and each set of spectra took at least 12 h to accumulate. All angular scans presented went through the $\langle 1\,1\,0\rangle$ axis on a line 14° from a $\{1\,1\,0\}$ plane.

As mentioned earlier, the beam halo that strikes the target holder was the major source of background. Background spectra were acquired using only a gold support ring without a crystal mounted. Without a target in the beam, the count rate was extremely low and therefore these spectra were integrated for 53 h. No single photon annihilation peaks were observed in the singles spectrum (no coincidence requirement). The coincidence spectrum, however, was subtracted from the spectra obtained with the Au crystal after being normalized to the number of positrons that struck the sample holder. This correction to the two-photon annihilation yield was ~20% in a random direction and as high as ~40% in the channeling direction. All data presented here have had this background subtracted.

To facilitate the comparison of spectra, they were normalized to the integrated number of positrons that impinged on the target. This was accomplished by normalizing at each angle with

$$N(\theta) = \frac{C_0}{C(\theta)} \int R(\theta)\,\mathrm{d}t, \tag{3}$$

where C_0 and $C(\theta)$ are counts in the beam dump scintillator in the channeling direction and at the desired angle, respectively. The instantaneous count rate in the beam dump is given by $R(\theta)$ and the integral is carried out over the running time of the experiment. The counting times for the ratio $C_0/C(\theta)$ was typically 50 s and was measured periodically. It was found to remain constant for a given θ and was proportional to the number of positrons impinging on the target. A scalar counted the positrons that hit the beam dump throughout the experiment and thereby calculated the integral of $R(\theta)$.

Fig. 4(a) shows the angular yields obtained from large angle scattering, two-photon annihilation and K-shell one-photon annihilation. Unfortunately, with this crystal thickness, the positron flux was too weak to produce observable L-shell or M-shell one-photon annihilation signals. The horizontal axis represents the angle between the positron beam and the $\langle 1\,1\,0\rangle$ axis of the crystal. The vertical axis is the observed yield normalized

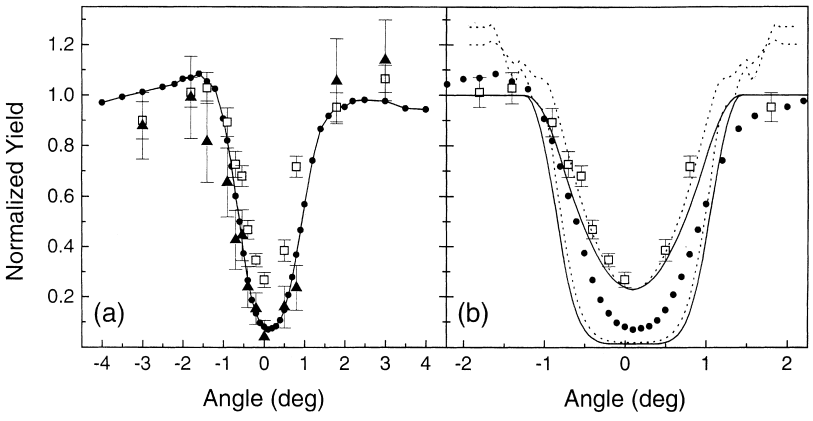

Fig. 4. (a) Normalized yield curves from 2.65 MeV positrons for large angle scattering (solid line with •), single photon annihilation (▲) and two-photon annihilation (□). Angle on horizontal axis measured from the $\langle 1\,1\,0\rangle$ axis of the 0.6 μm gold crystal. (b) Classical (solid line) and dynamical diffraction (dotted line) yield calculation of large angle scattering overlaid on the experimental data.

to unity for a non-channeling direction. For scattered positrons the on-axis minimum yield is 6.5% and the full width at half minimum of the channeling dip is 1.65°. The on-axis reduction of large angle nuclear scattering reflects the strong channeling suppression of the small impact parameter collisions ($b < 4 \times 10^{-3}$ Å) required for deflection to occur into the scattering detector. The relativistic critical angle for an axially channeled positron is given by

$$\theta_1 = \sqrt{\frac{2Ze^2}{\frac{1}{2}p_+ v_+ d}}, \tag{4}$$

where Z is the atomic number of the target, d the spacing of nuclei on the string and v_+ the velocity of the positron [33]. The expected width of the channeling dip is $2\theta_1$ but the large thermal vibrations in gold will reduce the width by a factor of ~0.8 [34]. For 2.65 MeV positrons along the $\langle 1\,1\,0\rangle$ axis in gold this expected width is 2.1°. The observed value is about 20% below this value. Discrepancies of this size have been seen before for channeled ions and positrons [20,35]. Furthermore, the widths from more detailed calculations are in better agreement (see below).

The similarity between the channeling yield curves for K-shell annihilation and large angle scattering may be understood by considering the K-shell Bohr radius ($a = 7 \times 10^{-3}$ Å), the scattering impact parameter ($b = 4 \times 10^{-3}$ Å) and the gold atomic thermal vibration amplitude ($\rho = 0.12$ Å). Since both processes require close proximity to the nucleus, i.e., smaller than the thermal vibration amplitude, it is expected that they exhibit very similar channeling characteristics. In comparison, the sensitivity of two-photon annihilation to the outer and valence electrons causes a striking difference. The full width is reduced to $1.25 \pm 0.09°$ and the minimum yield is four times higher at $27 \pm 3\%$. This is unambiguously attributed to the extended nature of the electron clouds around the nuclei and the delocalized electrons in the interstitial region. Since the single photon annihilation cross-section for these electrons is negligible, the smaller minimum yield of single versus two-photon annihilation verifies that annihilation with the outer and valence electrons is enhanced by the channeling process.

The theoretical description of channeled particles has been the subject of much investigation with both classical and quantum methods now well established. Fig. 4(b) shows classical and quantum mechanical yield calculations for large angle scattering and two-photon annihilation overlaid on the experimental data. The classical calculation (solid curves) uses a statistical equilibrium treatment of the channeling trajectories which are assumed to become ergodic and fill available phase-space. This calculational technique was first outlined in the seminal work by Lindhard [36]. The quantum calculation (dotted curves) is based on a dynamical diffraction formalism that successfully describes the well known phenomenon of electron channeling radiation [37]. The details of this method applied to the calculation of annihilation yields have been published by Hau et al. [17]. It should be noted that the same electron densities and potentials were used in both the calculations. They were calculated by a state-of-the-art augmented plane-wave method [38]. The quantum curves abruptly end at ±2° only because of the limits of our available computing power.

The quantum and classical calculation have strikingly similar widths with the quantum calculation narrower by ~6% and ~12% for scattering and annihilation, respectively. The shoulders starting at ±1.2° in the quantum curves arise because this calculation "obeys the rule of spatial averages" (e.g., the yield missing at small angles to an axis must be present as an excess at larger angles) [36]. This rule is violated by the statistical equilibrium technique used in the classical calculation. For large angle scattering, the calculated minimum yield is 2.0% with a width of 1.8°. The observed scattering width of 1.65° is only 8% below this calculated value but the observed minimum yield of 6.5% is 3.3 times larger than calculated. This is not surprising since the calculation does not include dechanneling effects. For two-photon annihilation the calculated full width agrees well with the annihilation data and qualitatively the shape agrees better than for the scattering curve. The calculated minimum yield is 14.5% in the absence of dechanneling. From the

observed scattering minimum yield we can estimate that dechanneling will increase the two-photon minimum yield to 23% which is 1.5 standard deviations from the experimentally observed value. The plotted annihilation yields include this correction.

Using these calculations we can also estimate the valence electron contribution. In gold we consider the valence electrons to be the 10 electrons in the 5d shell and the electron in the 6s shell. At large θ, where channeling does not occur, positrons penetrate into all regions of the crystal and therefore sample all electrons equally. Since there are 11 valence electrons, they constitute 14% of the total sampled at large θ. In contrast, channeled positrons are focused into the interstitial region where the valence electrons account for almost all of the electron density. Their annihilation contribution increases to 56% at minimum yield with the experimentally observed dechanneling correction included.

5. Conclusion

The observed larger channeling minimum yield for two-photon over one-photon annihilation confirms expectations that these channeling effects are very sensitive to electron density in the interstitial regions of crystals. Indeed the relative influence of valence electrons on channeling annihilation can be estimated to be about 10 times larger than the relative contribution of valence electrons to low order Fourier components of the charge density measured by X-ray diffraction techniques that have typically been used to determine electron densities in crystals [39].

It is also interesting to consider the spatial distribution in the classical versus quantum picture of channeling. Quantum effects have been seen in the momentum states of transmitted positrons for planar and axial channeling [16]. In contrast, angular yield measurements of close nuclear reaction processes appear classical in nature [20–23]. The quantum calculations presented here predict slightly narrower channeling widths because the quantum wavefunctions tunnel into classically forbidden regions of the channel. The difference between calculated widths is largest for two-photon annihilation which is also less sensitive to dechanneling processes. With better statistics from an intense beam this discrimination could be made.

It is the hope of the authors that the channeling phenomena revealed by this research will eventually result in an accurate easily applied probe of electrons in solid state materials. It is clear that higher positron beam currents are needed to perform experiments on a practical time scale; monoenergetic MeV positron beam currents greater than 10^7 e^+/s will be required. Stronger positron sources, improved moderators, polarization control, and more efficient detection and beam transport capabilities are possible with current technology. We believe that a serious discussion about combining these technologies into the next generation positron beam facility is needed. This new capability will also enable significant extensions of the experimental approach reported here. An intense MeV positron beam will allow the development of practical atomic scale channeling measurements of electronic spin densities [16,17], and momentum profiles in addition to valence and bonding electron density maps.

Acknowledgements

The authors would like to thank J. Chevalier, W. Gibson, R.A. Levesque, L.V. Hau, M. Weinert, and J.C. Palathingal for helpful contributions to this research. This work was supported by the National Science Foundation under contract DMR-9623610, the Norwegian Research Council and the Department of Energy through Lawrence Livermore National Laboratory under contract number W-7405-ENG-48.

References

[1] E. Bøgh, E. Uggerhøj, Phys. Lett. 17 (1965) 116.
[2] M.J. Alguard, R.L. Swent, R.H. Pantell, B.L. Berman, S.D. Bloom, S. Datz, Phys. Rev. Lett. 42 (1979) 1148.
[3] R.L. Swent, R.H. Pantell, M.J. Alguard, B.L. Berman, S.D. Bloom, S. Datz, Phys. Rev. Lett. 43 (1979) 1723.
[4] J.A. Golovchenko, A.N. Goland, J.S. Rosner, C.E. Thorn, H.E. Wegner, H. Knudsen, C.D. Moak, Phys. Rev. B 23 (1981) 957.

[5] S.P. Fomin, A. Jejcic, V.I. Kasilov, N.I. Lapin, J. Maillard, V.I. Noga, S.F. Shcherbak, N.F. Shul'ga, J. Silva, Nucl. Instr. and Meth. B 129 (1997) 29.
[6] L.C. Feldman, J.W. Mayer, S.T. Picraux, Materials Analysis by Ion Channeling: Submicron Crystallography, Academic Press, New York, 1982.
[7] B.Y. Tsaur, J.C.C. Fan, T.T. Sheng, Appl. Phys. Lett. 38 (1981) 447.
[8] P.G. Evans, O.D. Dubon, J.F. Chervinsky, F. Spaepen, J.A. Golovchenko, Appl. Phys. Lett. 73 (1998) 3120.
[9] J.U. Andersen, O. Andreasen, J.A. Davies, E. Uggerhøj, Radiat. Eff. 7 (1971) 25.
[10] S.T. Picraux, W.L. Brown, W.M. Gibson, Phys. Rev. B 6 (1972) 1382.
[11] B.R. Appleton, C. Erginsoy, H.E. Wegner, W.M. Gibson, Phys. Lett. 19 (1965) 185.
[12] W.M. Gibson, J.B. Rasmussen, P. Ambrosius-Olesen, C.J. Andreen, Can. J. Phys. 46 (1968) 551.
[13] G.R. Piercy, F. Brown, J.A. Davies, M. McCargo, Phys. Rev. Lett. 10 (1963) 399.
[14] S. Andriamonje, B. Blank, R.D. Moral, J.P. Dufour, L. Faux, A. Fleury, M.S. Pravikoff, C. Röhl, M. Chevallier, D. Dauvergne et al., Nucl. Instr. and Meth. B 87 (1994) 116.
[15] J.U. Andersen, J. Chevallier, G.C. Ball, W.G. Davies, J.S. Forster, J.S. Geiger, Phys. Rev. A 54 (1996) 624.
[16] R. Haakenaasen, L.V. Hau, J.A. Golovchenko, J.C. Palathingal, J.P. Peng, P. Asoka-Kumar, K.G. Lynn, Phys. Rev. Lett. 75 (1995) 1650.
[17] L.V. Hau, J.A. Golovchenko, R. Haakenaasen, A.W. Hunt, J.P. Peng, P. Asoka-Kumar, K.G. Lynn, M. Weinert, J.C. Palathingal, Nucl. Instr. and Meth. B 119 (1996) 30.
[18] L.V. Hau, A.W. Hunt, J.A. Golovchenko, R. Haakenaasen, K.G. Lynn, in: Y.C. Jean, M. Eldrup, D.M. Schrader, R.N. West (Eds.), Proceeding of the 11th International Conference on Positrons Annihilation, Trans Tech Publications, Switzerland, 1997.
[19] R. Haakenaasen, A.W. Hunt, J.A. Golovchenko, R.H. Howell, F.A. Selim, K.G. Lynn, T.E. Cowan, L.V. Hau, in: Y.C. Jean, M. Eldrup, D.M. Schrader, R.N. West (Eds.), Proceeding of the 11th International Conference on Positrons Annihilation, Trans Tech Publications, Switzerland, 1997.
[20] J.U. Andersen, W.M. Augustyniak, E. Uggerhøj, Phys. Rev. B 3 (1971) 705.
[21] E. Uggerhøj, Phys. Lett. 22 (1966) 382.
[22] E. Uggerhøj, J.U. Andersen, Can. J. Phys. 46 (1968) 543.
[23] P.J. Schultz, L.R. Logan, T.E. Jackman, J.A. Davies, Phys. Rev. B 38 (1988) 6369.
[24] L.A. Page, Phys. Rev. 106 (1957) 394.
[25] R.N. West, Adv. Phys. 22 (1973) 263.
[26] P. Hautojärvi, Positrons in Solids, no. 12 in Topics in Current Physics, Springer, Berlin, 1979.
[27] P.J. Schultz, K.G. Lynn, Rev. Mod. Phys. 60 (1988) 701.
[28] P. Asoka-Kumar, K.G. Lynn, D.O. Welch, J. Appl. Phys. 76 (1994) 4935.
[29] R.H. Howell, P.A. Sterne, M.J. Fluss, J.H. Kaiser, K. Kitazawa, H. Kojima, Phys. Rev. B 49 (1994) 13127.
[30] F.A. Selim, PhD thesis, Alexandria University, Egypt, 1999.
[31] J.A. Ferry, J.J. Kolonko, S.H. Phillips, S.J. Lundstrum, Nucl. Instr. and Meth. B 64 (1992) 309.
[32] J.C. Palathingal, P. Asoka-Kumar, K.G. Lynn, X.Y. Wu, Phys. Rev. A 51 (1995) 2122.
[33] P. Lervig, J. Lindhard, V. Nielsen, Nucl. Phys. A 96 (1967) 481.
[34] J.U. Andersen, Kgl. Danske Videnskab. Selskab Mat.-Fys. Medd. 36 (7) (1967).
[35] S.T. Picraux, J.A. Davies, L. Eriksson, N.G.E. Johansson, J.W. Mayer, Phys. Rev. 180 (1969) 873.
[36] J. Lindhard, Kgl. Danske Videnskab. Selskab Mat.-Fys. Medd. 34 (14) (1965).
[37] J.U. Andersen, E. Bonderup, E. Lægsgaard, B.B. Marsh, A.H. Sørensen, Nucl. Instr. and Meth. 194 (1982) 209.
[38] A.K. Rajagopal, Theory of Inhomogeneous Electron Systems: Spin-Density-Functional Formalism, no. 41 in Advances in Chemical Physics, Wiley, New York, 1980.
[39] B. Dawson, Proc. R. Soc. Lond. A 298 (1967) 379.